

2018. This manuscript version is made available under the CC-BY-NC-ND  
4.0 license  
<http://creativecommons.org/licenses/by-nc-nd/4.0/>

# Do meteoritic silicon carbide grains originate from asymptotic giant branch stars of super-solar metallicity?

Maria Lugaro<sup>a,b,\*</sup>, Amanda I. Karakas<sup>b,c</sup>, Mária Pető<sup>a</sup>, Emese Plachy<sup>a</sup>

<sup>a</sup>*Konkoly Observatory, Research Centre for Astronomy and Earth Sciences, Hungarian Academy of Sciences, H-1121 Budapest, Hungary*

<sup>b</sup>*Monash Centre for Astrophysics, School of Physics and Astronomy, Monash University, VIC 3800, Australia*

<sup>c</sup>*Research School of Astronomy and Astrophysics, Australian National University, Canberra, ACT 2611, Australia*

---

## Abstract

We compare literature data for the isotopic ratios of Zr, Sr, and Ba from analysis of single meteoritic stardust silicon carbide (SiC) grains to new predictions for the *slow* neutron-capture process (the *s* process) in metal-rich asymptotic giant branch (AGB) stars. The models have initial metallicities  $Z = 0.014$  (solar) and  $Z = 0.03$  (twice-solar) and initial masses 2 - 4.5  $M_{\odot}$ , selected such as the condition  $C/O > 1$  for the formation of SiC is achieved. Because of the higher Fe abundance, the twice-solar metallicity models result in a lower number of total free neutrons released by the  $^{13}\text{C}(\alpha, n)^{16}\text{O}$  neutron source. Furthermore, the highest-mass (4 - 4.5  $M_{\odot}$ ) AGB stars of twice-solar metallicity present a milder activation of the  $^{22}\text{Ne}(\alpha, n)^{25}\text{Mg}$  neutron source than their solar metallicity counterparts, due to cooler temperatures resulting from the effect of higher opacities. They also have a lower amount of the  $^{13}\text{C}$  neutron source than the lower-mass models, following their smaller He-rich region. The combination of these different effects allows our AGB models of twice-solar metallicity to provide a match to the SiC data without the need to consider large variations in the features of the  $^{13}\text{C}$  neutron source nor neutron-capture processes different from the *s* process. This raises the question if the AGB parent stars of meteoritic SiC

---

\*Maria Lugaro

Email address: [maria.lugaro@csfk.mta.hu](mailto:maria.lugaro@csfk.mta.hu) (Maria Lugaro)

grains were in fact on average of twice-solar metallicity. The heavier-than-solar Si and Ti isotopic ratios in the same grains are in qualitative agreement with an origin in stars of super-solar metallicity because of the chemical evolution of the Galaxy. Further, the SiC dust mass ejected from C-rich AGB stars is predicted to significantly increase with increasing the metallicity.

---

## 1. Introduction

Stardust grains are tiny specks of stars that formed in the winds of evolved stars and in the ejecta from supernova and nova explosions. They were injected in the interstellar medium and travelled to the birthplace of the Solar System, where they were incorporated into the parent bodies of meteorites. They are now extracted from meteorites and analysed via high-precision mass spectrometry. Their isotopic composition is an accurate record of the nuclear reactions that occurred in the deep, hot, dense layers of their parent stars and of the mixing processes that carried such material to the external regions where dust forms (Zinner, 2014).

Among stardust, silicon carbide (SiC) grains originate from a variety of sources, including supernovae (Pignatari et al., 2013) and novae (José et al., 2016), with the vast majority (> 90%, the “mainstream” SiC) from C-rich asymptotic giant branch (AGB) stars, based on their light (e.g., C, Ne, Si) and heavy elements (e.g., Sr, Zr, Ba) isotopic composition. SiC dust particles are predicted to form (Ferrarotti and Gail, 2006; Nanni et al., 2013; Dell’Agli et al., 2015) and are observed to be present around AGB stars (e.g., Speck et al., 2005). Furthermore, the isotopic signatures of meteoritic SiC grains qualitatively agree with those expected from nuclear reactions and mixing in these stars (Hoppe and Ott, 1997; Lugaro et al., 1999). In particular, mainstream SiC grains show the indisputable signature of *slow* neutron captures (the *s* process) in their parent stars: isotopes that are produced exclusively or predominately by the *s* process are found to be enhanced in these grains (Lugaro et al., 2003a). For example, SiC carry the famous Xe-S component, which shows excesses in  $^{128}\text{Xe}$

and  $^{130}\text{Xe}$  that can only be produced by the  $s$  process (Srinivasan and Anders, 1978).

It is well known observationally that the  $s$  process occurs in AGB stars (Merrill, 1952; Smith and Lambert, 1990). These stars are the final fate of stars with initial masses between roughly 1 and 8  $M_{\odot}$ , corresponding to the evolution that follows the exhaustion of both H and He in their cores (Karakas and Lattanzio, 2014). Energy is generated in AGB stars by the alternate nuclear burning of H and He in shells located in the deep layers of the star, just on top of the C-O degenerate core. The AGB evolution ends once the whole H-rich envelope is lost due to strong stellar winds and the core is left as a cooling white dwarf. On the AGB, H-burning is activated most of the time, while He-burning happens periodically on a short timescale of the order of 100 yr (thermal pulse, TP) and drives a convective region over the whole He-rich region located in-between the two burning shells. Such energetic but brief He-burning episodes result in the production of  $^{12}\text{C}$  from the triple- $\alpha$  reaction, whereas there is little production of  $^{16}\text{O}$ . The entire He-rich region becomes strongly enriched in  $^{12}\text{C}$  ( $\simeq 25\%$ , by mass fraction). The recurrent mixing episodes (the third dredge-up, TDU) that may follow each TP carry some of this material to the convective envelope, which can result in the envelope becoming C-rich and consequently in C-rich stellar outflows, a necessary condition for the formation of SiC.

In an AGB star, the  $s$  process occurs in the He- and C-rich region located between the H-burning shell and the He-burning shell. This is because  $\alpha$ -particles are required to drive the activation of the neutron source reactions,  $^{13}\text{C}(\alpha, n)^{16}\text{O}$  and  $^{22}\text{Ne}(\alpha, n)^{25}\text{Mg}$ . The largest uncertainty in current models is related to the availability of  $^{13}\text{C}$  in the low-mass ( $< 4 M_{\odot}$ ) AGB stars. These stars are observed to be strongly enriched in  $s$ -process elements (Busso et al., 2001), however, they do not reach the temperatures in excess of 300 MK needed to significantly activate the  $^{22}\text{Ne}(\alpha, n)^{25}\text{Mg}$  reaction. Accordingly, a relatively large number of  $^{13}\text{C}$  nuclei is required to release enough neutrons and drive the production of the bulk of the  $s$ -process abundances (Gallino et al., 1998; Goriely and Mowlavi, 2000; Lugaro et al., 2003b; Karakas and Lattanzio, 2007;

Cristallo et al., 2009). To solve this problem some mixing mechanism is assumed to occur at the end of each TDU episode and carry protons from the convective envelope into the He- and C-rich region. Reactions between the  $^{12}\text{C}$  nuclei and the protons lead to the production of  $^{13}\text{C}$  within a thin ( $\simeq 10^{-4} - 10^{-3} M_{\odot}$ ) region of the He-rich shell: the  $^{13}\text{C}$  “pocket”. Subsequently, the  $^{13}\text{C}(\alpha, n)^{16}\text{O}$  reaction releases neutrons during the H-burning phase, i.e., over long timescales ( $\sim 10^4$  yr) in radiative conditions before the onset of the next He-burning TP (Straniero et al., 1995).

If the temperature in TPs exceeds 300 MK the  $^{22}\text{Ne}(\alpha, n)^{25}\text{Mg}$  reaction also releases some free neutrons during convective He-shell burning. Fewer free neutrons are produced this way because the temperature in low-mass AGB stars may exceed 300 MK only in a few TPs and for short times,  $\sim 10$  yr. However, the  $^{22}\text{Ne}$  neutron source still affects the final *s*-process abundances because it releases neutron over the whole TP-driven convective zone, of mass  $\sim 20$  times larger than the  $^{13}\text{C}$  pocket, and produces local neutron densities up to five orders of magnitudes higher than the  $^{13}\text{C}$  neutron source (e.g., van Raai et al., 2012; Fishlock et al., 2014). This drives the opening of *branching points* at unstable nuclei along the *s*-process path with half lives longer than roughly one day, which can strongly modify the local isotopic pattern.

Within this framework, data for bulk SiC (e.g., Ávila et al., 2013) and for single SiC obtained via Resonant Ionization Mass Spectrometry (RIMS, e.g., Liu et al., 2014b) have been used to constrain various features of the modelling of the *s* process in AGB stars. Examples include nuclear reaction cross sections, both neutron-capture cross sections (e.g., Lugaro et al., 2003a) and neutron source reaction rates, especially the  $^{22}\text{Ne}(\alpha, n)^{25}\text{Mg}$  reaction (e.g., Liu et al., 2015), the mass range of the grain parent stars (Lugaro et al., 2003a), and the size of the  $^{13}\text{C}$  pocket and the efficiency of the neutron flux within it (Liu et al., 2014b,a, 2015). Noticeably, not only the mixing mechanism driving the formation of the  $^{13}\text{C}$  pocket is still under debate but also the uncertain effect of rotation on the operation of the  $^{13}\text{C}$  pockets (Herwig et al., 2003; Siess et al., 2004; Piersanti et al., 2013). The Zr, Sr, and Ba isotopic ratios measured in

single grains (Liu et al., 2014b,a, 2015) are particularly effective to constrain the neutron flux in the  $^{13}\text{C}$  pocket. This is because a number of isotopic ratios for these elements essentially depend on the *neutron exposure*, i.e., the time-integrated total number of free neutrons released in the  $^{13}\text{C}$  pocket. This in turn depends on the formation and the activation of the  $^{13}\text{C}$  neutron source itself.

It has been demonstrated that AGB stellar models of metallicity around solar and mass in the range for which C>O is achieved, i.e., around 2 - 4  $M_{\odot}$ , are not able to cover the isotopic spread observed in SiC grains, unless a large variety of  $^{13}\text{C}$ -pocket sizes and  $^{13}\text{C}$ -abundance profiles is considered (Lugaro et al., 2003a; Liu et al., 2014b,a, 2015). The need for such a spread of  $^{13}\text{C}$  pocket features has been supported by the discovery that metallicity variations could not be at the origin of the observed variations in the Zr, Sr, and Ba isotopic ratios (as was proposed by Lugaro et al., 2014). This is because there is no correlation between such ratios and the Si isotopic ratios (Liu et al., 2015), which are an independent metallicity indicator according to the chemical evolution of the Galaxy due to the fact that the production of  $^{29,30}\text{Si}$  in massive stars increases with the stellar metallicity, while the production of  $^{28}\text{Si}$  does not (Timmes and Clayton, 1996; Lewis et al., 2013).

One potential problem is that self-consistent investigations of the effect of the initial stellar mass and metallicity have been so far limited to metallicities around solar (defined here to be  $Z = 0.014$  following Asplund et al., 2009). Comparisons have been made with models of metallicities higher than solar from the FRUITY database (Cristallo et al., 2009, 2011) but only by up to 50% higher, i.e.,  $Z = 0.02^1$  (Liu et al., 2014b, 2015). The main reason for this is that AGB models of higher metallicity were not yet available. A new set of such models has recently been published by Karakas (2014) and the nucleosynthesis has been presented in Karakas and Lugaro (2016). Here we aim at exploring the comparison of predictions from these models to the composition of Zr, Sr, and

---

<sup>1</sup>close to the old value for the solar metallicity  $Z \approx 0.019$  (Anders and Grevesse, 1989).

Ba in single SiC grains. Our aim is to confirm if mass and metallicity variations cannot explain the range of the SiC grain data and consequently large variations in the features and/or operation of the  $^{13}\text{C}$  pocket are the only viable way to explain the observations. The paper is structured as follows: in Sec. 2 we describe our computational method and present the stellar evolutionary sequences. In Sec. 3 we present our model predictions for the Zr, Sr, and Ba isotopic ratios and compare them to the single grain data. In Sec. 4 we highlight the main consequences of our results and discuss arguments for and against the idea of invoking an origin of stardust grains in stars of twice-solar metallicity in the wider context of galactic evolution and SiC dust formation around C-rich AGB stars.

## 2. Stellar models

Karakas and Lugaro (2016) presented a large set of nucleosynthesis models for AGB stars in the mass range 1 to  $8 M_{\odot}$  for solar ( $Z = 0.014$ ), half-solar ( $Z = 0.007$ ), and twice-solar ( $Z = 0.03$ ) metallicity, the latter being the first published set of full AGB evolution and nucleosynthesis models at such metallicity. From that paper, we selected a subset of models of solar and twice-solar metallicity that become C-rich, the condition to form SiC molecules and dust. We selected the initial mass range from 2 to  $4.5 M_{\odot}$  because below  $2 M_{\odot}$  the TDU is typically not efficient enough to produce a C-rich envelope. Among the  $Z = 0.014$  models of Karakas and Lugaro (2016) the  $2 M_{\odot}$  star becomes C-rich without using overshoot, while for the lower masses convective overshoot is required. In the  $Z = 0.03$  models, convective overshoot is required for the models of  $M = 2.5 - 3 M_{\odot}$  to become C-rich (as discussed below). Above  $4.5 M_{\odot}$  our stellar models experience H burning at the base of the convective envelope (“hot bottom burning”), which destroys C and makes the star retain an O-rich envelope (e.g., Ventura et al., 2013).

In Table 1 we list for the selected models the main AGB model features that are of interest here. More physical properties of the selected models can be found

Table 1: Selected features of the stellar models: the number of thermal pulses (No. TP), the total mass dredged-up ( $M_{\text{TDU}}$ ), the maximum temperature reached during TPs ( $T_{\text{TP}}^{\text{max}}$ , which controls the activation of the  $^{22}\text{Ne}(\alpha, n)^{25}\text{Mg}$  neutron source), the number of thermal pulses during which the envelope is C-rich (No. TP with  $\text{C/O} > 1$ ), the final C/O ratio ( $\text{C/O}_{\text{fin}}$ ), and our standard choice of the extension in mass of the partial mixing zone (PMZ) leading to the formation of the  $^{13}\text{C}$  pocket in our models ( $M_{\text{PMZ}}$ , as described in detail in Sec. 2.1).

| Mass ( $M_{\odot}$ )  | No. TP | $M_{\text{TDU}}$ ( $M_{\odot}$ ) | $T_{\text{TP}}^{\text{max}}$ (MK) | No. TP<br>with $\text{C/O} > 1$ | $\text{C/O}_{\text{fin}}$ | $M_{\text{PMZ}}$ ( $M_{\odot}$ )<br>standard |
|-----------------------|--------|----------------------------------|-----------------------------------|---------------------------------|---------------------------|--|
| $Z = 0.014, Y = 0.28$ |        |                                  |                                   |                                 |                           |  |
| 2.00                  | 25     | 0.024                            | 280                               | 2                               | 1.16                      | $2 \times 10^{-3}$                           |
| 3.00                  | 28     | 0.099                            | 302                               | 10                              | 2.28                      | $2 \times 10^{-3}$                           |
| 4.00                  | 23     | 0.088                            | 348                               | 8                               | 1.75                      | $1 \times 10^{-3}$                           |
| 4.50                  | 31     | 0.096                            | 356                               | 1                               | 1.16                      | $1 \times 10^{-4}$                           |
| $Z = 0.03, Y = 0.30$  |        |                                  |                                   |                                 |                           |  |
| 2.50 <sup>a</sup>     | 30     | 0.060                            | 282                               | 1                               | 1.08                      | $2 \times 10^{-3}$                           |
| 2.75 <sup>b</sup>     | 33     | 0.073                            | 289                               | 2                               | 1.15                      | $2 \times 10^{-3}$                           |
| 3.00 <sup>c</sup>     | 33     | 0.071                            | 294                               | 2                               | 1.10                      | $2 \times 10^{-3}$                           |
| 3.50                  | 33     | 0.112                            | 308                               | 6                               | 1.30                      | $1 \times 10^{-3}$                           |
| 4.00                  | 24     | 0.083                            | 324                               | 1                               | 1.06                      | $1 \times 10^{-3}$                           |
| 4.50                  | 20     | 0.040                            | 335                               | 0                               | 0.76                      | $1 \times 10^{-4}$                           |

a) The base of the envelope was extended by  $N_{\text{ov}} = 2.5$  pressure scale heights

b)  $N_{\text{ov}} = 2.0$

c)  $N_{\text{ov}} = 1.0$

in Table 1 of Karakas (2014) and Table 1 of Karakas and Lugaro (2016). The structure models with  $Z = 0.03$  and initial mass 2.5, 2.75, and 3  $M_{\odot}$  included here were recomputed by Karakas and Lugaro (2016) including overshoot at the base of the convective envelope in order for the models to become C-rich. To include overshoot during the TDU the base of the envelope was extended by  $N_{\text{ov}}$  pressure scale heights (Karakas et al., 2010; Kamath et al., 2012), using the value reported in the footnotes of Table 1 for each model and keeping it constant along the whole AGB evolution. Including overshoot, the lowest calculated initial mass



at which an AGB star becomes C-rich at  $Z = 0.03$  moves down from 3.25 to 2.5  $M_{\odot}$ . As the stellar mass increases,  $T_{\text{TP}}^{\text{max}}$  also increases and reaches above 300 MK for masses greater than  $\simeq 3 M_{\odot}$ . This effect depends on the metallicity, for the same initial mass AGB stars with  $Z = 0.03$  are generally cooler due to the higher opacities. Note that in our models we do not include overshoot at the base of the TP-driven convective zone. This leads to (1) higher abundances of  $^{12}\text{C}$  in the He-rich region, hence higher  $^{13}\text{C}$  abundances and a more efficient neutron flux in the  $^{13}\text{C}$  pocket, and (2) higher temperatures in the TP-driven convective zone, leading to a stronger activation of the  $^{22}\text{Ne}$  neutron source (Lugaro et al., 2003b). Pignatari et al. (2016) and Battino et al. (2016) have recently presented a selection of AGB s-process models including such overshoot and it will be interesting in the future to compare predictions from these models to the stardust SiC data.

Finally, we note that we do not include core overshooting during the main sequence and core He burning phases of our model stars. For a given initial mass, this would increase the core mass at the beginning of the AGB, somewhat decreasing the maximum initial mass for which a C-rich AGB star is obtained (since hot bottom burning would operate at a lower initial mass). However, we do not consider this uncertainty since it has a similar effect as, e.g., the convective model used on the AGB (e.g., Ventura and D’Antona, 2005). Observations of AGB stars and planetary nebulae have helped constrain the mass range for C-rich stars to  $\sim 1.5$  to  $\sim 3\text{--}4 M_{\odot}$  in the Magellanic Clouds (Frogel et al., 1990; Lattanzio and Wood, 2003). For the Galaxy the exact range is more uncertain due to the distance determinations, but still consistent with an upper limit  $\sim 4 M_{\odot}$  (Guandalini and Cristallo, 2013).

### *2.1. The post-processing step and the formation of the $^{13}\text{C}$ pocket*

Our computational method involves two steps: first we calculated the stellar evolutionary sequences described above from the main sequence to near the tip of the AGB, and second we fed the stellar structure inputs ( $T$ ,  $\rho$ , and convective velocities) into a post-processing code that solves simultaneously the abundance

changes due to nuclear reactions and to convective mixing for 328 nuclear species from neutrons and protons to Pb and Bi. The stellar models are described in detail in Karakas (2014). The nucleosynthesis models and their results are described in detail in Karakas and Lugaro (2016)<sup>2</sup>.

The bulk of the 2351 nuclear reactions in the post-processing code comes from the JINA reaclib database, as of May 2012. Of specific interest here are the neutron source reactions  $^{13}\text{C}(\alpha, n)^{16}\text{O}$  and  $^{22}\text{Ne}(\alpha, n)^{25}\text{Mg}$ , from Heil et al. (2008) and Iliadis et al. (2010), respectively. For the neutron-capture reactions we selected those labelled “ka02” in the JINA reaclib, since they provide us with the best fits of the *kadonis.org* database (Dillmann et al., 2006) at the temperatures of interest for AGB stars. For the Zr isotopes we took the values from Lugaro et al. (2014). We implemented in the network the temperature dependence of a number of  $\beta$ -decay rates following the compilation of Takahashi and Yokoi (1987) (see details in Karakas and Lugaro, 2016). Of specific interest here is the inclusion of the temperature dependence of the  $\beta^-$ -decay rates of  $^{134,135,136,137}\text{Cs}$ , which are required to calculate accurate Ba isotopic ratios.

In the post-processing, we need to increase the abundance of the main neutron source  $^{13}\text{C}$  in the He-rich region to obtain models that are rich in *s*-process elements (e.g., Gallino et al., 1998; Goriely and Mowlavi, 2000). In order to do this, we artificially partially mix protons from the convective envelope into the radiative He-rich shell at the time of the deepest extent of each TDU episode by imposing a parametrized proton profile. The depth over which protons are mixed into the He-intershell is referred to as the “partial mixing zone” (hereafter PMZ). In all our models we use an exponential proton profile to describe how much material is mixed from the envelope into the He-rich region down to

---

<sup>2</sup>While Karakas (2014) presented stellar structure models also with variable initial He abundance, Karakas and Lugaro (2016) only considered the models with canonical initial He abundances (as defined by Karakas, 2014). The detailed nucleosynthesis of the models with different He abundances and the implications on the comparison with the composition of SiC stardust will be the subject of future studies.

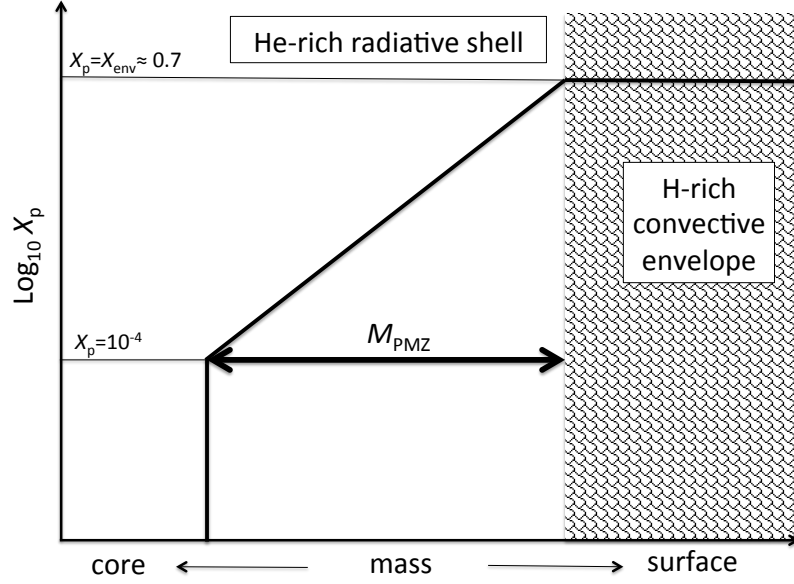


Figure 1: Schematic diagram illustrating the proton profile implemented for the PMZ leading to the formation of the  $^{13}\text{C}$  pockets in our models. The proton mass fraction at each mass point  $m$  belonging to the PMZ is simply given by  $X_p = f(m) \times X_{\text{env}}$ , where the function  $f(m) = 10^{-m}$ ,  $X_{\text{env}}$  is the envelope abundance, and the equation is normalised such as at the top of the PMZ,  $X_p = X_{\text{env}}$  and at the bottom,  $X_p = 10^{-4}$  (below which value the  $s$ -process is inefficient). Note that this description involves three free parameters:  $M_{\text{PMZ}}$ , the  $10^{-4}$  value at the bottom of the PMZ, and the function  $f(m)$ . Of these here we only vary  $M_{\text{PMZ}}$  (decreasing the  $10^{-4}$  value at the bottom of the PMZ is equivalent to decreasing  $M_{\text{PMZ}}$ ). The effect of varying the function  $f(m)$  have been shown to not be very significant (Goriely and Mowlavi, 2000) in changing the abundance distribution.

a given mass extent,  $M_{\text{PMZ}}$  (Fig. 1).

We stress that our insertion of the PMZ during the post-processing is not implemented via an overshoot process where the diffusive coefficient (Herwig, 2000) or the velocity (Cristallo et al., 2009) are decayed exponentially beyond the formal convective border leading to the partial mixing. Instead, it represents directly the final result of such kind of overshoot. This “exponential” overshoot differs from the overshoot that we have implemented in the stellar structure code described above to force a deeper TDU. In the stellar structure code, we extended the position of the base of the convective envelope by  $N_{\text{ov}}$  pressure-scale heights and used homogeneous mixing in the overshoot region. This does not lead to the *partial* mixing required for the formation of the PMZ, but to instantaneous *complete* mixing of the region added to the convective envelope via the TDU.

Our choice of an exponential profile is consistent with profiles resulting from more self-consistent models for the formation of the  $^{13}\text{C}$  pocket, for example, those that involve the “exponential” overshoot mentioned above or gravity waves (Denissenkov and Tout, 2000), while it differs from the profile of Trippella et al. (2016), which is based on mixing induced by magnetic fields and results in lower local abundances of  $^{13}\text{C}$ . Once the mixing profile is set, the main factor that controls the local  $^{13}\text{C}$  and  $^{14}\text{N}$  abundances in each layer of the pocket are the proton-capture rates of  $^{12}\text{C}$  and  $^{13}\text{C}$ . Where the  $p/^{12}\text{C}$  ratio is below  $\simeq 0.04$ , all the protons are consumed by the  $^{12}\text{C}(p,\gamma)^{13}\text{N}(\beta^+)^{13}\text{C}$  reaction chain and there are none left to destroy  $^{13}\text{C}$  via  $^{13}\text{C}(p,\gamma)^{14}\text{N}$ . This results in the formation of the pocket rich in  $^{13}\text{C}$ . Where the  $p/^{12}\text{C}$  ratio is above  $\simeq 0.04$ , the  $^{13}\text{C}(p,\gamma)^{14}\text{N}$  is also activated producing a region rich in  $^{14}\text{N}$  instead (Goriely and Mowlavi, 2000; Lugaro et al., 2003b; Cristallo et al., 2009). The final resulting  $s$ -process distribution is determined essentially by the local  $^{13}\text{C}$  and  $^{14}\text{N}$  abundances in each mass layer of the pocket. In fact, for AGB stars of mass below  $\sim 5 M_{\odot}$ , where the  $s$  process is dominated by the  $^{13}\text{C}$  pocket, our final results are in good agreement with the results from the FRUITY database (Cristallo et al., 2011, 2015), a consequence of the similar proton profile (for a detailed comparison see

Lugaro et al., 2012; Fishlock et al., 2014; Karakas and Lugaro, 2016).

In the models presented in Karakas and Lugaro (2016) and here, we vary only one of the free parameters related to our description of the  $^{13}\text{C}$  pocket: the depth reached by the partial mixing, in other words, the extent in mass involved in the mixing,  $M_{\text{PMZ}}$ . As described at length in Karakas and Lugaro (2016), we define our standard choice for this parameter by decreasing its value as the initial stellar mass increases (see Table 1). For stars of mass  $M \leq 3 M_{\odot}$  we set  $M_{\text{PMZ}} = 2 \times 10^{-3} M_{\odot}$ , which is reduced to  $1 \times 10^{-3} M_{\odot}$  for stars of mass  $3 M_{\odot} < M \leq 4 M_{\odot}$ , and then reduced further to  $1 \times 10^{-4} M_{\odot}$  for  $4 M_{\odot} < M < 5 M_{\odot}$ . For stars above  $5 M_{\odot}$  we set  $M_{\text{PMZ}} = 0$ , that is, we assume that  $^{13}\text{C}$  pockets do not form. These choices reflect the shrinking in mass of the He-rich intershell region with increasing stellar mass: smaller  $^{13}\text{C}$  pockets are found in intermediate-mass models by more self-consistent models because of the steeper step in the pressure profile between the core and the envelope (Cristallo et al., 2009). Furthermore, our choice for stars above  $5 M_{\odot}$  accounts for the theoretical prediction that  $^{13}\text{C}$  pockets are small or do not form when the base of the convective envelope is hot during the TDU (Goriely and Siess, 2004). This is also in line with the observational constraint that the effect of the  $^{13}\text{C}$  neutron source disappears as the AGB mass increases (García-Hernández et al., 2013). In Karakas and Lugaro (2016) we provided the results obtained by experimenting with varying  $M_{\text{PMZ}}$ . Here we do the same for three selected  $Z = 0.03$  models, and with the choices of  $M_{\text{PMZ}}$  reported in Figure 3. These experiments are needed given the current limitations of our models. First, our standard choice of the variation of  $M_{\text{PMZ}}$  with the stellar mass is quite crude. Second, in our models  $M_{\text{PMZ}}$  is kept constant over the whole evolution of the star. This is in contrast with the finding of Cristallo et al. (2009) that the extent in mass of the  $^{13}\text{C}$  pocket decreases along the AGB evolution for any given model, due to the shrinking of the He-rich region, as in the case of the more massive stars. Experimenting with  $M_{\text{PMZ}}$  provides us with a simple method to explore beyond such limitations.

Our models do not include stellar rotation or magnetic fields. All stars rotate

and this can have a strong effect on the  $s$  process because rotation in the core can generate mixing inside the  $^{13}\text{C}$  pocket and carry  $^{14}\text{N}$  in the  $^{13}\text{C}$ -rich region. Nitrogen-14 is a strong neutron poison with a relatively high neutron-capture cross section of  $\simeq 3$  mbarn (Wallner et al., 2016). It steals free neutrons from the Fe seeds, and in the presence of  $^{14}\text{N}$  the production of  $s$ -process elements is somewhat inhibited. Rotation is a 3D phenomenon and its implementation in 1D stellar models relies on simplifications, which limit our understanding of the mixing instabilities that can result from it (Maeder, 2009). One recent example is the work of Caleo et al. (2016), who demonstrated that the Goldreich-Schubert-Fricke instability is not as efficient as so far assumed. Not surprisingly, while all studies of rotational mixing in AGB stars agree that it affects the  $s$  process, quantitative results vary widely, from a strong (Herwig et al., 2003; Siess et al., 2004) to a mild (Piersanti et al., 2013) suppression of the  $s$  process, depending on the implementation and the input physics. Furthermore, the angular momentum distribution within a giant star can be affected by magnetic fields, either already present in stars (Maeder and Meynet, 2014) or generated by rotation itself (Spruit, 2002; Cantiello et al., 2014), by gravity waves (Fuller et al., 2014), and by mixed oscillation modes (Belkacem et al., 2015). These effects generally result in the spin down of the core in giant stars and core He-burning stars that is clearly required by asteroseismology observations (Mosser et al., 2012; Deheuvels et al., 2015). The first consequence is that stars should reach the AGB with a radial differential rotation weaker than predicted by models including rotation only. Furthermore, similar effects may play a role also during the AGB phase to extract angular momentum from the core. Overall, the discontinuity of the angular momentum at the location of the  $^{13}\text{C}$  pocket may be smaller, driving less rotational mixing than predicted by models including rotation only. Detailed models are required to quantitatively test the potential outcome. On the other hand, magnetic fields may lead to other types of mixing instabilities (Nucci and Busso, 2014).

In the context of all these uncertainties, our models, which do not include any of the effects mentioned above, are useful as a baseline to understand which

of the potential effects on mixing in the  $^{13}\text{C}$  pocket, among rotation, magnetic fields, gravity waves, and mixed oscillations, need to be considered to match the observations. Meteoritic stardust grains in this respect play a crucial role in improving our understanding of AGB stars. However, to be able to use stardust grains as a discriminant for the model uncertainties we need first to ascertain the mass and metallicity of their parent stars.

### 3. Results

We present the comparison between our model results and the single grain RIMS data in three separate subsections, dedicated to Zr, Sr, and Ba, respectively, and with a final fourth subsection showing the comparison to the correlated measurements of Sr and Ba presented by Liu et al. (2015). We employ the  $\delta$ -value notation to represent the isotopic ratios, i.e., the permil variation with respect to the solar ratio (for which  $\delta=0$ ), which we use as initial in the models<sup>3</sup>. In each subsection we present two types of plots: the first type compares our AGB models of solar metallicity and twice-solar metallicity to the stardust data. All the models listed in Table 1 are plotted in these figures, including the  $Z = 0.03$  model of initial mass  $4.5 M_{\odot}$ , which does not become C-rich. We include it nevertheless to illustrate the predicted trend with increasing mass from 4 to  $4.5 M_{\odot}$  for such metallicity. Stars in this mass region are still candidate grain parent stars within the model uncertainties because they represent the transition phase between the C-rich low-mass AGB stars and the massive AGB stars that remain O-rich. These stars may remain O-rich because of the effect of hot bottom burning and/or the combined effect of a larger envelope mass and less material dredged up from the He-rich intershell (owing to the shrinking in mass of the He-shell with increasing stellar mass). The final composition of the model also depends on the choice of the AGB mass-loss rate, which is uncertain

---

<sup>3</sup>Different initial isotopic ratios would not affect the final results, which are dominated by the *s*-process production.

and determines the overall AGB lifetime. In our AGB models we use the semi-empirical mass-loss rate formula proposed by Vassiliadis and Wood (1993) based on observations of the correlation between the mass loss and pulsation period. Several others are available in the literature, both theoretical and empirical (for a recent discussion see, e.g., Rosenfield et al., 2014).

In more detail, the  $4.5 M_{\odot}$   $Z = 0.014$  model experiences a relatively weak hot bottom burning (with a maximum temperature at the base of the convective envelope of 63 MK), which allows the envelope to become C-rich. In contrast, the  $4.5 M_{\odot}$   $Z = 0.03$  model does not experience hot bottom burning but does not become C-rich due to the lower amount of TDU and the higher amount of initial O compared to its  $Z = 0.014$  counterpart. However, at the point where our calculations stopped converging after 20 TPs (as compared to 31 TPs for the  $Z = 0.014$  case) the mass of the envelope was still  $0.9 M_{\odot}$ . A few more TDU episodes, which are well within model uncertainties, may allow this model to become C-rich, making it a potential candidate for producing SiC grains.

The second type of plot within each subsection focuses instead on a selection of models with twice-solar metallicity and initial masses 3, 3.5, and  $4 M_{\odot}$  to illustrate the effect of changing the mass extent of the partial mixing zone,  $M_{\text{PMZ}}$ . Note that varying the extent of the PMZ does not change the relative local  $^{13}\text{C}$  and  $^{14}\text{N}$  abundance profiles. These profiles, together with the metallicity, control the neutron exposure in the pocket, which, in turn, controls the *relative* abundance distribution in the pocket. However, because the same abundance profiles are extended or squeezed in a wider or thinner mass region, varying  $M_{\text{PMZ}}$  affects the *absolute* abundances produced, which, in turn, determines how far the predicted isotopic ratios shift away from their initial solar values. Nevertheless, some feedback between this effect and those related to the mass and metallicity of the star is present in some cases. Note that the C/O ratios at the stellar surface mildly decrease with increasing  $M_{\text{PMZ}}$  because of the destruction of  $^{12}\text{C}$  in the He-rich region resulting in the formation of the  $^{13}\text{C}$  pocket and the production of  $^{16}\text{O}$  due to the activation of the  $^{13}\text{C}(\alpha, n)^{16}\text{O}$  reaction. This is why the models with larger  $M_{\text{PMZ}}$  may show one or two less



TPs with  $C/O > 1$  than the models with smaller  $M_{\text{PMZ}}$ .

To interpret the model predictions we need to keep in mind the two main differences resulting from increasing the metallicity from solar to twice solar. The first is the difference in the amount of Fe, which increases for higher metallicities and leads to a lower neutron exposure in the  $^{13}\text{C}$  pocket (Clayton, 1988). This mostly affects the ratios of isotopes with magic ( $^{88}\text{Sr}/^{86}\text{Sr}$  and  $^{138}\text{Ba}/^{136}\text{Ba}$ ) or close-to-magic ( $^{90,91,92}\text{Zr}/^{94}\text{Zr}$ ) number of neutrons. The second is the different stellar structure that results from the higher opacities, which make the star generally cooler at higher metallicities. We note that the models of  $Z = 0.03$  presented by Lugaro et al. (2014) were calculated by changing the metallicity only during the post-processing because the self-consistent stellar models of  $Z = 0.03$  were not yet available. The  $Z = 0.03$  models presented in Lugaro et al. (2014) did not capture all the effects described above and their interplay as done here.

### 3.1. Zr

The left panels of Figure 2 show the predictions for the solar metallicity models and demonstrate two well known results (Lugaro et al., 2003a, 2014; Liu et al., 2014a). (1) Only stellar model of  $\leq 3 M_{\odot}$  can be considered as potential parent stars of the SiC grains. Stars of initial mass above  $3 M_{\odot}$  experience temperatures up to 360 MK during the thermal pulses (Table 1), which activate the  $^{22}\text{Ne}(\alpha, n)^{25}\text{Mg}$  reaction. This results in high neutron density and an overproduction of  $^{96}\text{Zr}$  relative to the grain data: the predicted  $^{96}\text{Zr}/^{94}\text{Zr}$  ratio is higher, rather than lower than solar as observed in the grains. (2) The models cannot cover the grains with  $^{90,91,92}\text{Zr}/^{94}\text{Zr}$  ratios close to solar. To achieve a match large variations need to be assumed for both the size and the detailed abundance profiles in the  $^{13}\text{C}$  pocket (Liu et al., 2014a).

The right panels of Figure 2 show the predictions for the twice-solar metallicity models. The situation here is very different. Stars of mass  $\leq 3 M_{\odot}$  produce results quite similar to their solar-metallicity counterparts, however, models of mass greater than  $3 M_{\odot}$  are also potentially good candidates to be parent

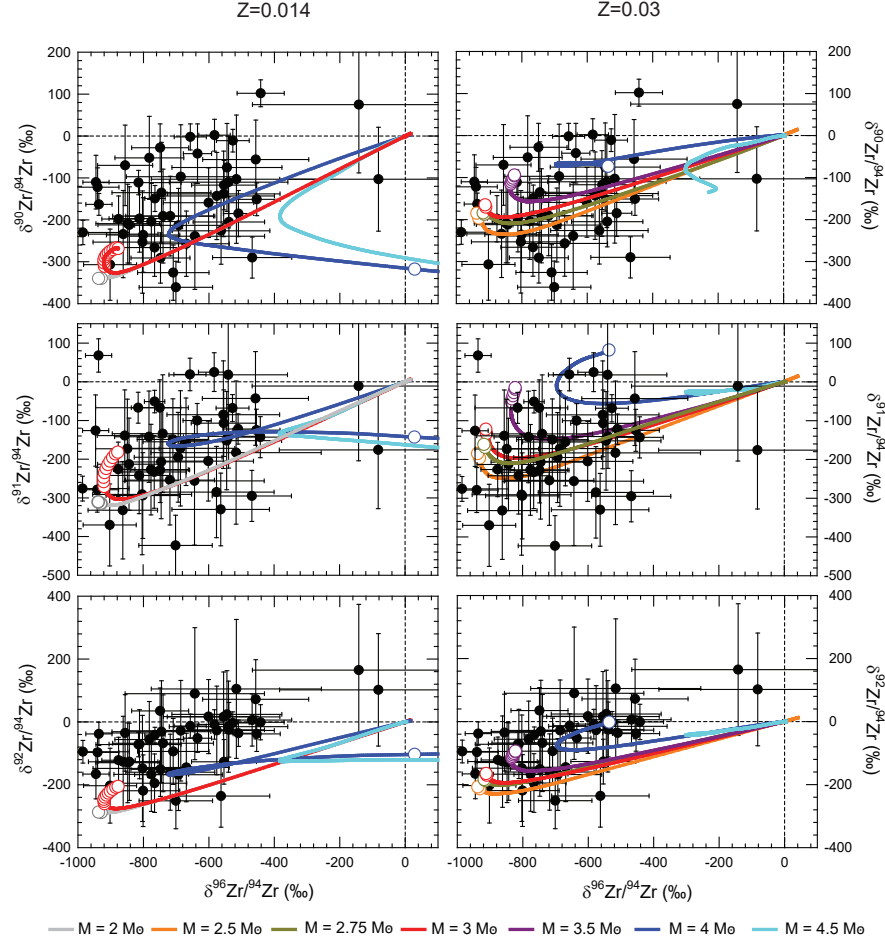


Figure 2: The RIMS SiC grains data for Zr (black circles with  $2\sigma$  error bars, for references see Liu et al., 2014a) are compared to the surface evolution of stellar models of solar metallicity (left panel) and of twice-solar metallicity (right panel) of different masses from 2 to  $4.5 M_{\odot}$  and our standard choice of the  $M_{\text{PMZ}}$  parameter (Table 1). The dashed lines represent the solar composition with  $\delta = 0$  by definition. Each coloured line represents the evolution of a different initial mass and open circles on the lines represent the TDE during which  $C/O > 1$  in the envelope.



stars of the grains. In fact, stars of initial mass between 3 and 4  $M_{\odot}$  provide a good match to the grains showing  $^{90,91,92}\text{Zr}/^{94}\text{Zr}$  ratio close to solar, which are not covered by the models of solar metallicity. The twice-solar metallicity stars are cooler than their solar metallicity counterparts, which means that the  $^{22}\text{Ne}(\alpha, n)^{25}\text{Mg}$  reaction is not as efficiently activated and the  $^{96}\text{Zr}/^{94}\text{Zr}$  ratio remains negative as seen in the grains. On the other hand, the  $^{13}\text{C}$  pocket is smaller in models of  $M \geq 3 M_{\odot}$ . This means that the  $^{22}\text{Ne}$  neutron source has a larger relative weight on the determination of the final surface abundances. One of the effects is to re-adjust the  $^{92}\text{Zr}/^{94}\text{Zr}$  ratio to its equilibrium value given by the inverse ratio of the neutron-capture rates at the temperature at which the  $^{22}\text{Ne}$  source is activated ( $\sim 300$  MK), higher than that at which the  $^{13}\text{C}$  source is activated ( $\sim 90$  MK). Because the neutron-capture rate of  $^{92}\text{Zr}$  decreases as the temperature increase, this results in higher  $^{92}\text{Zr}/^{94}\text{Zr}$  ratios during the activation of the  $^{22}\text{Ne}$  neutron source (Liu et al., 2014a). The combination of these effects results in a bending of the evolutionary curves for the 3.5 and 4  $M_{\odot}$   $Z = 0.03$  models that is more pronounced than in the lower masses, but not as large as in the solar metallicity models of similar mass.

All previous studies had difficulties in predicting solar values of  $^{92}\text{Zr}/^{94}\text{Zr}$ . For example, changes in the neutron-capture cross sections (Lugaro et al., 2003a), not confirmed by recent experiments (Tagliente et al., 2010), or large variations in the size of the  $^{13}\text{C}$  pocket had to be invoked. Liu et al. (2014a) assumed a smaller  $^{13}\text{C}$  pocket in low-mass AGB stars of solar/subsolar metallicity to enhance the imprint of the  $^{22}\text{Ne}$  neutron source. This effect naturally occurs in our 4  $M_{\odot}$   $Z = 0.03$  model once we assume that the PMZ is smaller in extent than in models of lower mass. We stress that in our models this assumption was made *a priori*, based on the stellar structure (i.e., following the reduced mass of the He-rich region) and from the independent observational evidence described in Sec. 2.

In Figure 3 we experimented with varying the extent of the PMZ within the selected  $Z = 0.03$  models. The effects are not large, although they help to cover the spread in  $^{96}\text{Zr}/^{94}\text{Zr}$ . If we increase the extent of the PMZ in the 4  $M_{\odot}$

models the  $^{96}\text{Zr}$  is higher than observed in the majority of the grains, although it would cover the two unusual grains with composition close to solar.

In summary, our analysis of the Zr isotopic ratios demonstrates the strong effect of the stellar evolutionary model on the predicted surface isotopic composition. Models of higher metallicity experience lower He-shell burning temperatures and a lower activation of the  $^{22}\text{Ne}$  neutron source so that  $^{96}\text{Zr}$  is not overproduced. The other important factor is the decrease of the extent in mass of the He-rich shell (which controls the extent in mass of the  $^{13}\text{C}$  pocket) as the stellar mass increases. Taking into account natural variations of the stellar mass in the  $Z = 0.03$  models allows us to predict the whole range of Zr isotopic ratios presented by the grains. Only a small fraction of the grains, those with the lowest  $^{90,91,92}\text{Zr}/^{94}\text{Zr}$  ratios show the signature of a possible origin in AGB stars of solar metallicity, but these models do not appear to be absolutely necessary in order to cover the data. On average, the models produce  $^{90,91}\text{Zr}/^{94}\text{Zr}$  ratios  $\sim 10\%$  higher than observed, this is within the  $2\sigma$  uncertainties in the neutron-capture cross sections (Tagliente and et al., 2008b,a). The behaviour of the theoretical evolution lines is strongly affected by the potential variations of the neutron-capture rates of  $^{90,91,92,94}\text{Zr}$  with temperature. Note that the accuracy of the predicted abundance of  $^{96}\text{Zr}$  is determined by the neutron-capture cross section of the branching point isotope  $^{95}\text{Zr}$ , which is still debated and needs to be tested further. Furthermore different values have been proposed for the rate of the neutron source reaction  $^{22}\text{Ne}(\alpha, n)^{25}\text{Mg}$ , which is affected by potential systematic uncertainties (Bisterzo et al., 2015; Massimi and et al., 2017). These nuclear uncertainties will be considered in forthcoming work.

### 3.2. Sr

The top and middle left panels of Figure 4 demonstrate the effect on the  $^{88}\text{Sr}/^{86}\text{Sr}$  ratios of increasing the stellar metallicity. An increase in metallicity lowers the overall neutron exposure, because of the increase in the number of Fe seeds, which results in a lower  $^{88}\text{Sr}/^{86}\text{Sr}$  ratio. A small number of grains show  $^{88}\text{Sr}/^{86}\text{Sr}$  ratios that are higher than solar, which is expected from solar

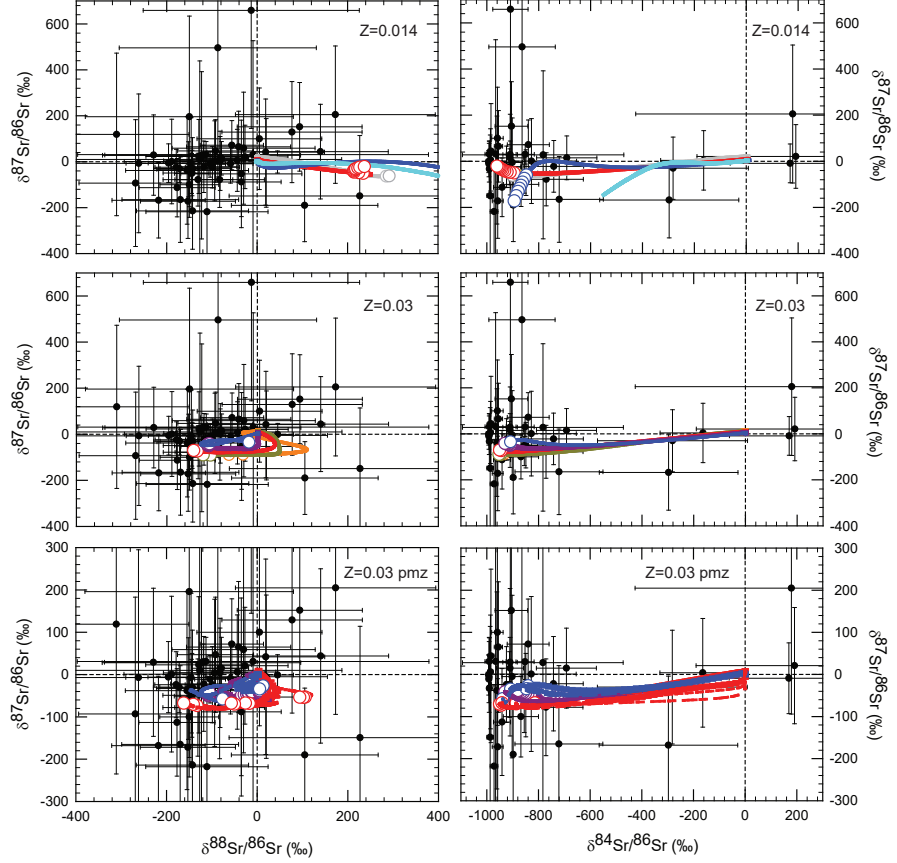


Figure 4: As in Figure 2, the RIMS SiC grains data for Sr from Liu et al. (2015) (black circles with  $2\sigma$  error bars) are compared to the surface evolution of stellar models of solar metallicity (top panel) and of twice-solar metallicity (middle panel) of different masses from 2 to  $4.5 M_{\odot}$  and our standard choice of the  $M_{\text{PMZ}}$  parameter. Open circles on the lines represent the TDUs when the envelope reaches  $C/O > 1$ . In the bottom panels (zoomed-in) we show the selection of  $Z = 0.03$  models with varying  $M_{\text{PMZ}}$ , as in Figure 3. Since  $^{84}\text{Sr}$  is not included in our full network, we calculated  $\delta(^{84}\text{Sr}/^{86}\text{Sr})$  by assuming that the initial surface abundance of  $^{84}\text{Sr}$  does not change, since  $^{84}\text{Sr}$  is completely destroyed by neutron captures in the intershell. This approximation is valid within roughly 10 permil.

metallicity models, although the error bars are very large. The bulk of the grains instead present  $^{88}\text{Sr}/^{86}\text{Sr}$  ratios that are lower than solar, as predicted by the twice-solar metallicity models. On the other hand, mass and metallicity do not play a major role in the determination of the  $^{84}\text{Sr}/^{86}\text{Sr}$  ratio, since  $^{84}\text{Sr}$  is destroyed by neutron captures and its abundance does not significantly change at the stellar surface, and the  $^{87}\text{Sr}/^{86}\text{Sr}$  ratio, which is mostly defined by the local equilibrium abundances controlled by the neutron-capture cross sections of  $^{86}\text{Sr}$  and  $^{87}\text{Sr}$ . Uncertainties in these neutron-capture cross sections need to be tested (see discussion in Liu et al., 2015), especially given that the latest measurements are relatively old (Bauer et al., 1991). Variations in the extent of the PMZ (bottom panel of Figure 4) do not result in major changes. Overall, in agreement with the Zr comparison, Sr also indicates that AGB stars of twice-solar metallicity are good potential candidates as the site of origin of most of the SiC grains.

### 3.3. Ba

Figure 5 shows that the models of twice-solar metallicity provide an overall better match also when considering the Ba data. The  $^{134}\text{Ba}/^{136}\text{Ba}$  ratios predicted for the low-mass ( $< 4 M_{\odot}$ ) stars are similar for the two metallicities. However, the higher-mass stars of twice-solar metallicity show a more prominent decrease of the  $^{134}\text{Ba}/^{136}\text{Ba}$  ratio. If we consider the whole range of masses down to the  $4.5 M_{\odot}$  model, which as discussed above may be borderline in becoming C-rich, the negative  $\delta(^{134}\text{Ba}/^{136}\text{Ba})$  values observed in the grains are reached, down to  $-200$ , and possibly lower if the evolution was extended with a few more TDU episodes. This is due to the enhanced relative impact of the  $^{22}\text{Ne}(\alpha, n)^{25}\text{Mg}$  reaction on the overall final abundances (similarly to the case of  $^{92}\text{Zr}/^{94}\text{Zr}$  discussed above), which leaves a stronger imprint of the activation of the  $^{134}\text{Cs}$  branching point. For grains with significantly negative  $\delta(^{134}\text{Ba}/^{136}\text{Ba})$ , Liu et al. (2014b) invoked a process different from the  $s$  process: the intermediate neutron-capture ( $i$ ) process driven by proton ingestion episodes in the late thermal pulses in post-AGB stars. Here we propose that  $\simeq$

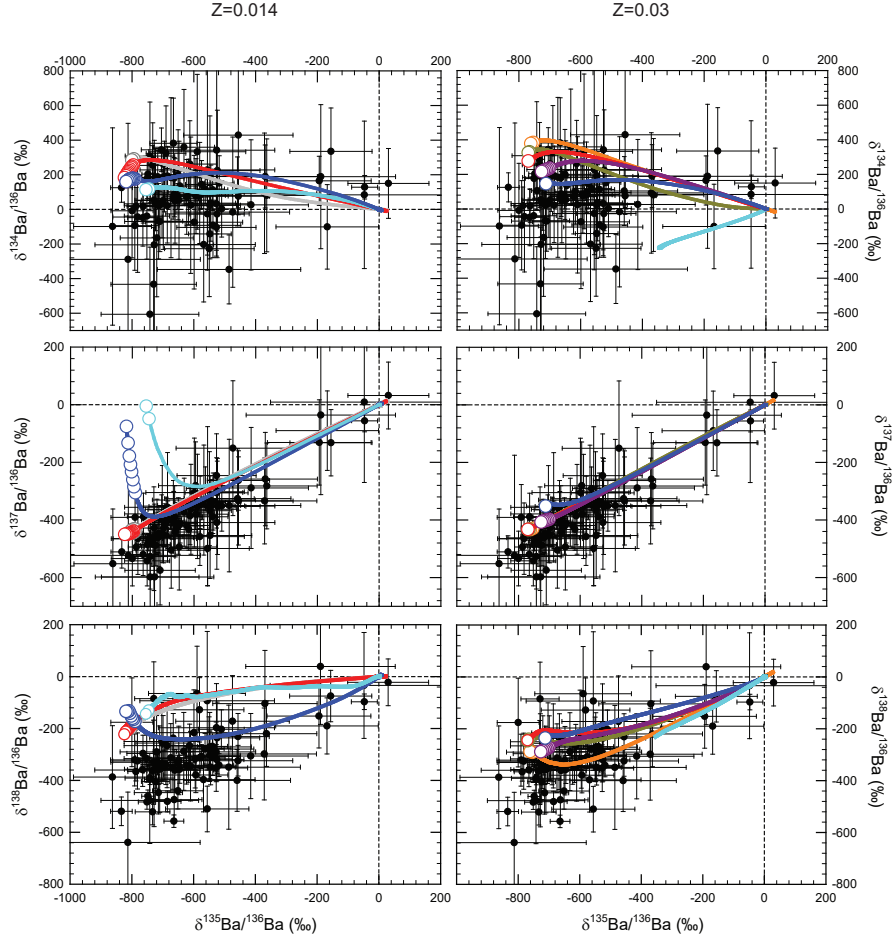


Figure 5: Same as Figure 2, for the Ba isotopic ratios and with SiC grains RIMS data for Ba from Liu et al. (2014b) and Liu et al. (2015) (black circles with  $2\sigma$  error bars, from which we excluded the grains classified as “contaminated” by Liu et al., 2015). Open circles on the lines represent the TDUs when the envelope reaches  $C/O > 1$ .



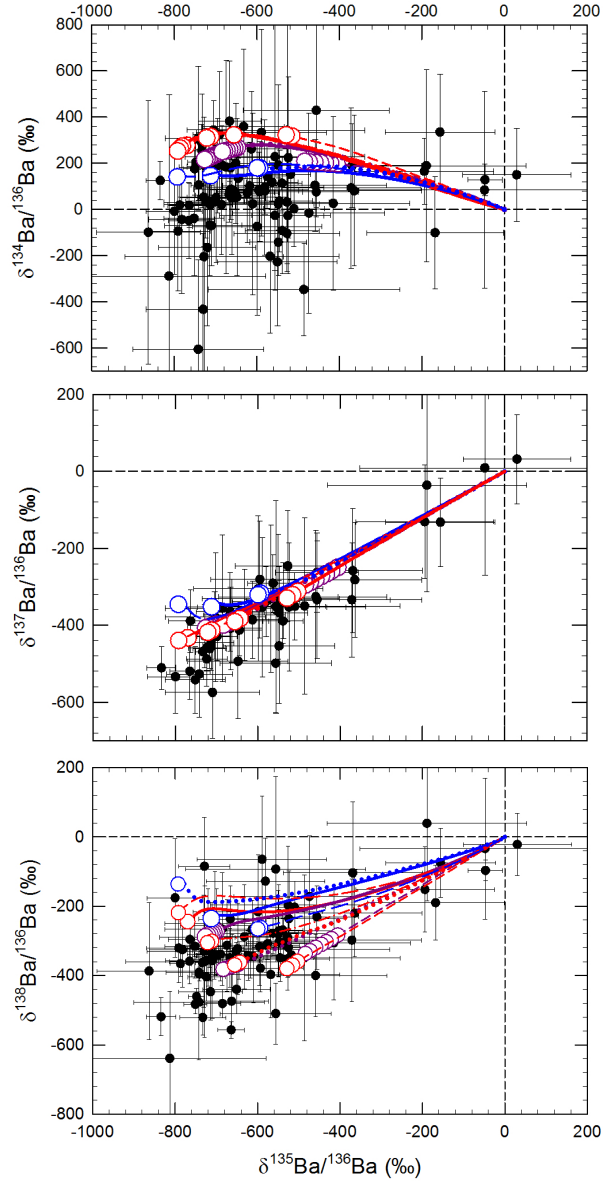


Figure 6: Same as Figure 3, for the Ba isotopic ratios.

4.5  $M_{\odot}$   $Z = 0.03$  C-rich AGB stars are the best candidates to be investigated for the origin of these grains. This is supported by the fact that the expected total dust yield for a post-AGB star is  $\sim 10^{-6} M_{\odot}$  (Karakas et al., 2015), three orders of magnitude lower than the expected SiC-only dust yield for C-rich AGB stars of metallicity solar to twice-solar (Ferrarotti and Gail, 2006; Nanni et al., 2013). We expect SiC grains from post-AGB stars to represent less than 0.1% of mainstream SiC grains.

The case of the  $^{137}\text{Ba}/^{136}\text{Ba}$  ratio is similar to that of the  $^{96}\text{Zr}/^{94}\text{Zr}$  ratio, where models of mass  $> 3 M_{\odot}$  at solar metallicity are excluded due to the activation of the branching points at  $^{134,135,136}\text{Cs}$ . On the other hand, all the masses at  $Z = 0.03$  are consistent with the data. Finally, similarly to the case of the  $^{88}\text{Sr}/^{86}\text{Sr}$  ratio, the effect of the lower neutron exposure in stars of twice-solar metallicity is to decrease the  $^{138}\text{Ba}/^{136}\text{Ba}$  ratios to the typical values seen in the grains, while the solar metallicity models produce ratios higher than observed.

Variations in  $M_{\text{PMZ}}$  (Figure 6) broaden the spread in  $^{135}\text{Ba}/^{136}\text{Ba}$ , which helps to cover the full set of data, and further decrease  $\delta(^{138}\text{Ba}/^{136}\text{Ba})$  to  $-400$ , in the case of the 3.5  $M_{\odot}$  model with  $M_{\text{PMZ}} = 2 \times 10^{-4} M_{\odot}$ , also helping to cover the whole of the observed range. Generally, as  $M_{\text{PMZ}}$  decreases the impact of the  $^{22}\text{Ne}$  neutron source increases. This neutron source is characterised by lower neutron exposures than the  $^{13}\text{C}$  neutron source, which results in material with lower  $^{138}\text{Ba}/^{136}\text{Ba}$  ratios. Overall, considering the Ba data we reach the same conclusion that AGB models with  $Z = 0.03$  produce a much better match than models of  $Z = 0.014$ . The handful of grains with  $\delta(^{134}\text{Ba}/^{136}\text{Ba}) \simeq -400$  and those with  $\delta(^{138}\text{Ba}/^{136}\text{Ba}) \simeq -500$  are not covered by the models. The role of uncertainties in the stellar models related to the efficiency of the TDU and the mass-loss need to be investigated in detail in relation to these specific grains, as well as the nuclear physics uncertainties related to the operation of the branching point at  $^{134}\text{Cs}$  and its temperature dependence, which controls the final  $^{134}\text{Ba}/^{136}\text{Ba}$  ratio.

### 3.4. *Sr versus Ba*

Since Sr and Ba data are available for the same single SiC grains (Liu et al., 2015) we are able to perform another self-consistency check using the observed correlation between the  $^{138}\text{Ba}/^{136}\text{Ba}$  versus  $^{88}\text{Sr}/^{86}\text{Sr}$ , which are both controlled mainly by the neutron exposure. Figure 7 confirms the compatibility of the data with the twice-solar metallicity models and the incompatibility with the solar metallicity models. As note above the only data not covered by the models are those with  $\delta(^{138}\text{Ba}/^{136}\text{Ba}) \simeq -500$ . Interestingly, these point appear to have higher than average  $\delta(^{88}\text{Sr}/^{86}\text{Sr})$  values, an effect related to the activation of the  $^{22}\text{Ne}$  source in our model, i.e., becoming more evident when  $M_{\text{PMZ}}$  is smaller ( $\sim 10^{-4} M_{\odot}$ ). This suggests that a possibility to explain these data may be a more efficient TDU combined with the smaller  $M_{\text{PMZ}}$ , detailed models are required to test this speculation.

## 4. Discussion

Our comparison of stardust SiC data with new AGB models shows that twice-solar metallicity models perform much better than solar metallicity models in covering self-consistently all the Zr, Sr, and Ba isotopic ratios. These metal-rich models can reach grains with  $^{90,91,92}\text{Zr}/^{94}\text{Zr}$  ratios close to solar and they produce the observed  $^{88}\text{Sr}/^{86}\text{Sr}$  and  $^{138}\text{Ba}/^{136}\text{Ba}$  ratios, without the need to invoke large variations in the features of the  $^{13}\text{C}$  pocket. Furthermore, twice-solar metallicity models with mass around  $4.5 M_{\odot}$  can potentially cover grains with  $^{134}\text{Ba}/^{136}\text{Ba}$  significantly lower than solar, which were not possible to explain before within the framework of the *s* process. Allowing for some variations in  $M_{\text{PMZ}}$  allow us a better coverage of the data, and it is potentially more realistic given the limitation of our models described in Sec. 2.

Our study demonstrates that the effect of metallicity alone on the Zr, Sr, and Ba isotopic ratios is not as simple as envisaged by Lugaro et al. (2014): not only the Fe seed abundance changes, affecting the neutron exposure, but also the stellar structure is modified. We have found that for C-rich AGB models

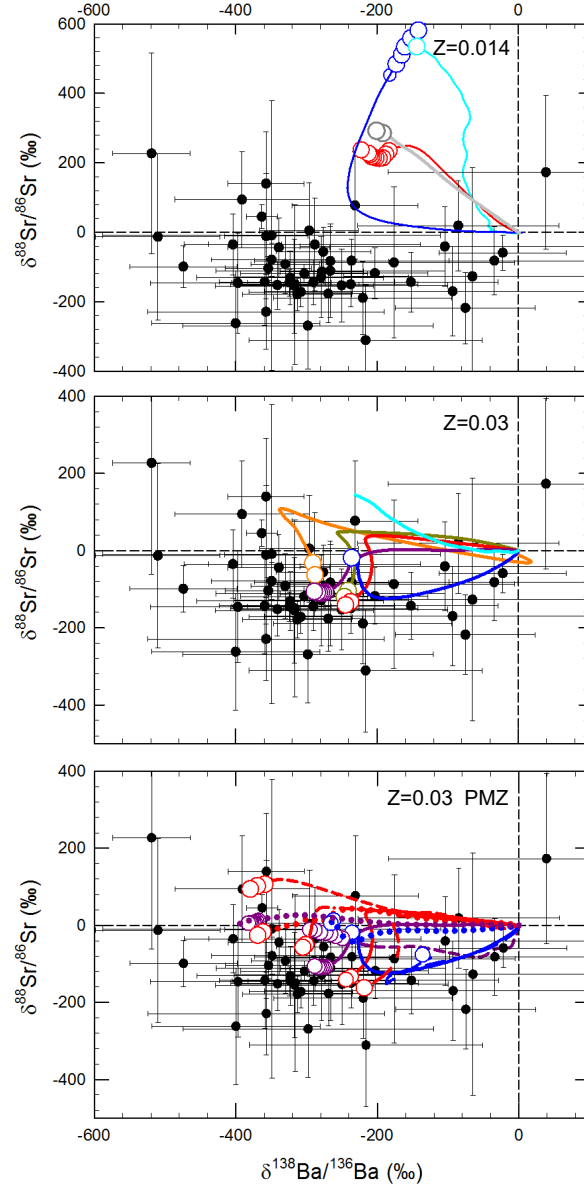


Figure 7: Same as Figure 4, for the correlated  $^{138}\text{Ba}/^{136}\text{Ba}$  versus  $^{88}\text{Sr}/^{86}\text{Sr}$  (from Liu et al., 2015, black circles with  $2\sigma$  error bars and excluding the grains classified as “contaminated”).

of twice-solar metallicity the initial stellar mass also plays an important role by modulating the interplay between the effect of the two neutron sources,  $^{13}\text{C}$  and  $^{22}\text{Ne}$ . In particular, most of the data can be covered using only models of twice-solar metallicity and masses from 2 to  $4.5 M_{\odot}$ . This means that it is not possible to attribute the spread in the isotopic ratios to metallicity only (Lugaro et al., 2014), because the stellar mass is an important second parameter. This is in agreement with the fact that Liu et al. (2015) did not find any correlation between the Sr and Ba isotopic ratios with the Si isotopic ratios, which are expected to depend on the initial metallicity of the star via the chemical evolution of the Galaxy (Timmes and Clayton, 1996; Lewis et al., 2013). It is also not possible to attribute the spread in the isotopic ratios to variations in the features of the  $^{13}\text{C}$  pocket only, because of the significant effects resulting from the combination of mass and metallicity we have found here.

From these results the main question arises: is it possible that meteoritic stardust SiC grains originated from AGB stars on average of twice-solar metallicity? The Si (and Ti) isotopic ratios of the grains represent another piece of evidence that can be used to answer this question. It is a well known and long-standing problem that the Si isotopic ratios in mainstream SiC grains are up to 20% larger than solar. This has been considered a puzzle for decades because according to models of the chemical evolution of the Galaxy the Si isotopic ratios increase with the metallicity in the Galaxy and in a simple model the metallicity should increase with the age of the Galaxy (e.g., Kobayashi et al., 2011). This means that the stars that produced the stardust grains that were trapped inside meteorites more than 4.6 billion years ago should have been born after the Sun, obviously a paradox (Timmes and Clayton, 1996).

However, this simple picture of Galactic chemical evolution has been challenged in recent years by observations of large stellar samples showing that there is no strong correlation between age and metallicity in the Galaxy and that stars exist that are older than the Sun but have higher metallicities. Recent large stellar surveys of the solar neighborhood show that stars with ages between that of

the Sun and roughly 9 Gyr<sup>4</sup> have a spread in metallicity from 0.2 to 2.5 of solar (Casagrande et al., 2011; Bensby et al., 2014). Such a large spread in metallicity is currently interpreted as the effect of stellar migration in the Galaxy (see, e.g., Spitoni et al., 2015, and references therein). Interestingly, Clayton (1997) already proposed that the distribution of the Si isotopic ratios in SiC could be interpreted via stellar migration. However, migration is not enough: Lewis et al. (2013) compared the average metallicity observed by the Geneva-Copenhagen stellar survey to that obtained from SiC grains using a detailed revision of the Galactic chemical evolution of the Si isotopes and concluded that the two do not match because the average metallicity of the parent stars of the SiC grains is twice as high as the average metallicity of stars of the required age range observed in the solar neighbourhood. They interpreted this finding by considering one more piece of the puzzle: that the efficiency of SiC dust production increases with metallicity. By comparing the stellar and the grain samples, Lewis et al. (2013) derived the relative formation efficiency for SiC as function of metallicity as a power-law, which predicts that AGB stars of twice-solar metallicity should produce roughly five times more SiC dust than AGB stars of solar metallicity. This is in agreement with detailed dust formation models (Ferrarotti and Gail, 2006).

With our present study, another problem has arisen: we have derived that the majority of SiC grains should have formed in AGB stars of metallicity twice-solar, while according to the updated Galactic chemical evolution models of the Si isotopes of Lewis et al. (2013) the majority of SiC grains should have formed in AGB stars of metallicity from solar to 70% above solar.

This result depends on a number of uncertainties, including the production of the silicon isotopes in supernovae, which is not well understood (Hoppe et al., 2009), the details of the chemical evolution of the Galaxy, and the fact that

---

<sup>4</sup>corresponding to the maximum age of a star that could have evolved in time to contribute SiC grains to the presolar nebula, assuming a minimum initial mass of 1.5  $M_{\odot}$  for an AGB star to become C-rich.

inhomogeneities in the interstellar medium can result in variations in the Si isotopic ratios of up to 5% (Lugaro et al., 1999; Nittler, 2005), to be added to the variation due to the chemical evolution of the Galaxy. It is also dependent on the exact values of the reference Solar System abundances, specifically for the abundant C, N, O, and Fe.

More dedicated studies are needed to address the question that we pose in the title of this paper. Specifically, detailed population synthesis models are required to compare models and data in a statistical fashion, especially to be able to exploit the large amount of data expected in the near future from the new CHILI RIMS instrument (Stephan et al., 2016). Statistical studies, coupled with a systematic analysis of the nuclear uncertainties will allow us to derive quantitatively the extent of the bias towards twice-solar metallicity stars for the origin of mainstream SiC that we propose here, and decide if this bias is feasible within our current knowledge of dust formation around AGB stars. Furthermore, we need to compare AGB models to observations for other elements, such as Gd and Dy (Ávila et al., 2016) and Fe and Ni (Trappitsch et al., 2016). More correlated RIMS investigations of different elements in the same grains will also help future investigations of the origin of mainstream SiC stardust.

## Acknowledgements

M. L. and A. I. K. acknowledge the mentoring of Ernst Zinner all through their career, and M. L. is particularly grateful for his encouragement during her PhD. Without his support none of our work on trying to elucidate the origin of stardust grains would have been possible. His inspiration will guide us further to answer the question of the origin of the grains. M. L. is a Momentum (“Lendület-2014” Programme) project leader of the Hungarian Academy of Sciences. M. L. and A. I. K. are grateful for the support of the NCI National Facility at the ANU. M. P. is a Research Fellow of the Hungarian Academy of Sciences. E. P. is supported by the Hungarian NKFIH Grants PD-121203 and K-115709.

## References

## References

- Anders, E., Grevesse, N., 1989. Abundances of the elements - meteoritic and solar. *Geochim. Cosmochim. Acta* 53, 197–214.
- Asplund, M., Grevesse, N., Sauval, A.J., Scott, P., 2009. The chemical composition of the Sun. *Ann. Rev. Astron. Astrophys.* 47, 481–522.
- Ávila, J.N., Ireland, T.R., Lugaro, M., Gyngard, F., Karakas, A., 2016. Gadolinium and dysprosium isotopic compositions in stardust SiC grains from the Murchison meteorite. *LPI Contributions* 1921, 6318.
- Ávila, J.N., Ireland, T.R., Lugaro, M., Gyngard, F., Zinner, E., Cristallo, S., Holden, P., Rauscher, T., 2013. Europium s-process signature at close-to-solar metallicity in stardust SiC grains from asymptotic giant branch stars. *Astrophys. J. Lett.* 768, L18.
- Battino, U., Pignatari, M., Ritter, C., Herwig, F., Denisenkov, P., Den Hartogh, J.W., Trappitsch, R., Hirschi, R., Freytag, B., Thielemann, F., Paxton, B., 2016. Application of a theory and simulation-based convective boundary mixing model for AGB star evolution and nucleosynthesis. *Astrophys. J.* 827, 30.
- Bauer, R.W., Bazan, G., Becker, J.A., Howe, R.E., Mathews, G.J., 1991. Neutron capture cross sections of  $^{86}\text{Sr}$  and  $^{87}\text{Sr}$  from 100 eV to 1 MeV, the conditions for the astrophysical *s* process, and the  $^{87}\text{Rb}$ - $^{87}\text{Sr}$  cosmochronometer. *Phys. Rev. C* 43, 2004–2011.
- Belkacem, K., Marques, J.P., Goupil, M.J., Mosser, B., Sonoi, T., Ouazzani, R.M., Dupret, M.A., Mathis, S., Grosjean, M., 2015. Angular momentum redistribution by mixed modes in evolved low-mass stars. II. Spin-down of the core of red giants induced by mixed modes. *Astron. Astrophys.* 579, A31.



- Bensby, T., Feltzing, S., Oey, M.S., 2014. Exploring the Milky Way stellar disk. A detailed elemental abundance study of 714 F and G dwarf stars in the solar neighbourhood. *Astron. Astrophys.* 562, A71.
- Bisterzo, S., Gallino, R., Käppeler, F., Wiescher, M., Imbriani, G., Straniero, O., Cristallo, S., Görres, J., deBoer, R.J., 2015. The branchings of the main s-process: Their sensitivity to  $\alpha$ -induced reactions on  $^{13}\text{C}$  and  $^{22}\text{Ne}$  and to the uncertainties of the nuclear network. *Mon. Not. R. Astron. Soc.* 449, 506–527.
- Busso, M., Gallino, R., Lambert, D.L., Travaglio, C., Smith, V.V., 2001. Nucleosynthesis and mixing on the asymptotic giant branch. III. Predicted and observed s-process abundances. *Astrophys. J.* 557, 802–821.
- Caleo, A., Balbus, S.A., Tognelli, E., 2016. The Goldreich-Schubert-Fricke instability in stellar radiative zones. *Mon. Not. R. Astron. Soc.* 460, 338–344.
- Cantiello, M., Mankovich, C., Bildsten, L., Christensen-Dalsgaard, J., Paxton, B., 2014. Angular momentum transport within evolved low-mass stars. *Astrophys. J.* 788, 93.
- Casagrande, L., Schönrich, R., Asplund, M., Cassisi, S., Ramírez, I., Meléndez, J., Bensby, T., Feltzing, S., 2011. New constraints on the chemical evolution of the solar neighbourhood and Galactic disc(s). Improved astrophysical parameters for the Geneva-Copenhagen Survey. *Astron. Astrophys.* 530, A138.
- Clayton, D.D., 1988. Nuclear cosmochronology within analytic models of the chemical evolution of the solar neighbourhood. *Mon. Not. R. Astron. Soc.* 234, 1–36.
- Clayton, D.D., 1997. Placing the Sun and mainstream SiC particles in galactic chemodynamic evolution. *Astrophys. J. Lett.* 484, L67–L70.
- Cristallo, S., Piersanti, L., Straniero, O., Gallino, R., Domínguez, I., Abia, C., Di Rico, G., Quintini, M., Bisterzo, S., 2011. Evolution, nucleosynthesis, and yields of low-mass asymptotic giant branch stars at different metallicities. II. The FRUITY database. *Astrophys. J. Suppl.* 197, 17.

- Cristallo, S., Straniero, O., Gallino, R., Piersanti, L., Domínguez, I., Lederer, M.T., 2009. Evolution, nucleosynthesis, and yields of low-mass asymptotic giant branch stars at different metallicities. *Astrophys. J.* 696, 797–820.
- Cristallo, S., Straniero, O., Piersanti, L., Gobrecht, D., 2015. Evolution, nucleosynthesis, and yields of AGB stars at different metallicities. III. Intermediate-mass models, revised low-mass models, and the ph-FRUITY interface. *Astrophys. J. Suppl.* 219, 40.
- Deheuvels, S., Ballot, J., Beck, P.G., Mosser, B., Østensen, R., García, R.A., Goupil, M.J., 2015. Seismic evidence for a weak radial differential rotation in intermediate-mass core helium burning stars. *Astron. Astrophys.* 580, A96.
- Dell’Agli, F., Ventura, P., Schneider, R., Di Criscienzo, M., García-Hernández, D.A., Rossi, C., Brocato, E., 2015. Asymptotic giant branch stars in the Large Magellanic Cloud: evolution of dust in circumstellar envelopes. *Mon. Not. R. Astron. Soc.* 447, 2992–3015.
- Denissenkov, P.A., Tout, C.A., 2000. On a physical mechanism for extra mixing in globular cluster red giants. *Mon. Not. R. Astron. Soc.* 316, 395–406.
- Dillmann, I., Heil, M., Käppeler, F., Plag, R., Rauscher, T., Thielemann, F.K., 2006. KADoNiS - The Karlsruhe astrophysical database of nucleosynthesis in stars, in: Woehr, A., Aprahamian, A. (Eds.), *Capture Gamma-Ray Spectroscopy and Related Topics*, pp. 123–127.
- Ferrarotti, A.S., Gail, H.P., 2006. Composition and quantities of dust produced by AGB stars and returned to the interstellar medium. *Astron. Astrophys.* 447, 553–576.
- Fishlock, C.K., Karakas, A.I., Lugaro, M., Yong, D., 2014. Evolution and nucleosynthesis of asymptotic giant branch stellar models of low metallicity. *Astrophys. J.* 797, 44.
- Frogel, J.A., Mould, J., Blanco, V.M., 1990. The asymptotic giant branch of Magellanic Cloud clusters. *Astrophys. J.* 352, 96–122.

- Fuller, J., Lecoanet, D., Cantiello, M., Brown, B., 2014. Angular momentum transport via internal gravity waves in evolving stars. *Astrophys. J.* 796, 17.
- Gallino, R., Arlandini, C., Busso, M., Lugaro, M., Travaglio, C., Straniero, O., Chieffi, A., Limongi, M., 1998. Evolution and nucleosynthesis in low-mass asymptotic giant branch stars. II. Neutron captures and the *s*-process. *Astrophys. J.* 497, 388.
- García-Hernández, D.A., Zamora, O., Yagüe, A., Uttenthaler, S., Karakas, A.I., Lugaro, M., Ventura, P., Lambert, D.L., 2013. Hot bottom burning and *s*-process nucleosynthesis in massive AGB stars at the beginning of the thermally-pulsing phase. *Astron. Astrophys.* 555, L3.
- Goriely, S., Mowlavi, N., 2000. Neutron-capture nucleosynthesis in AGB stars. *Astron. Astrophys.* 362, 599–614.
- Goriely, S., Siess, L., 2004. *S*-process in hot AGB stars: A complex interplay between diffusive mixing and nuclear burning. *Astron. Astrophys.* 421, L25–L28.
- Guandalini, R., Cristallo, S., 2013. Luminosities of carbon-rich asymptotic giant branch stars in the Milky Way. *Astron. Astrophys.* 555, A120.
- Heil, M., Käppeler, F., Uberseder, E., Gallino, R., Pignatari, M., 2008. Neutron capture cross sections for the weak *s* process in massive stars. *Phys. Rev. C* 77, 015808.
- Herwig, F., 2000. The evolution of AGB stars with convective overshoot. *Astron. Astrophys.* 360, 952–968.
- Herwig, F., Langer, N., Lugaro, M., 2003. The *s*-process in rotating asymptotic giant branch stars. *Astrophys. J.* 593, 1056–1073.
- Hoppe, P., Leitner, J., Meyer, B.S., The, L.S., Lugaro, M., Amari, S., 2009. An unusual presolar silicon carbide grain from a supernova: implications for

- the production of silicon-29 in Type II supernovae. *Astrophys. J. Lett.* 691, L20–L23.
- Hoppe, P., Ott, U., 1997. Mainstream silicon carbide grains from meteorites, in: Bernatowicz, T.J., Zinner, E. (Eds.), *Astrophysical Implications of the Laboratory Study of Presolar Materials*, pp. 27–58.
- Iliadis, C., Longland, R., Champagne, A.E., Coc, A., Fitzgerald, R., 2010. Charged-particle thermonuclear reaction rates: II. Tables and graphs of reaction rates and probability density functions. *Nuclear Physics A* 841, 31–250.
- José, J., Halabi, G.M., El Eid, M.F., 2016. Synthesis of C-rich dust in CO nova outbursts. *Astron. Astrophys.* 593, A54.
- Kamath, D., Karakas, A.I., Wood, P.R., 2012. Evolution and nucleosynthesis of AGB stars in three Magellanic Cloud clusters. *Astrophys. J.* 746, 20.
- Karakas, A.I., 2014. Helium enrichment and carbon-star production in metal-rich populations. *Mon. Not. R. Astron. Soc.* 445, 347–358.
- Karakas, A.I., Campbell, S.W., Stancliffe, R.J., 2010. Is extra mixing really needed in asymptotic giant branch stars? *Astrophys. J.* 713, 374–382.
- Karakas, A.I., Lattanzio, J.C., 2007. Stellar models and yields from asymptotic giant branch stars. *Publ. Astron. Soc. Aust.* 24, 103–117.
- Karakas, A.I., Lattanzio, J.C., 2014. The Dawes Review 2: Nucleosynthesis and stellar yields of low- and intermediate-mass single stars. *Publ. Astron. Soc. Aust.* 31, 30.
- Karakas, A.I., Lugaro, M., 2016. Stellar yields from metal-rich asymptotic giant branch models. *Astrophys. J.* 825, 26.
- Karakas, A.I., Ruiter, A.J., Hampel, M., 2015. R Coronae Borealis stars are viable factories of pre-solar grains. *Astrophys. J.* 809, 184.

- Kobayashi, C., Karakas, A.I., Umeda, H., 2011. The evolution of isotope ratios in the Milky Way galaxy. *Mon. Not. R. Astron. Soc.* 414, 3231–3250.
- Lattanzio, J.C., Wood, P.R., 2003. Evolution, nucleosynthesis, and pulsation of AGB stars, in: Habing, H.J., Olofsson, H. (Eds.), *Asymptotic giant branch stars*. Astronomy and astrophysics library, New York, Berlin: Springer, p. 23.
- Lewis, K.M., Lugaro, M., Gibson, B.K., Pilkington, K., 2013. Decoding the message from meteoritic stardust silicon carbide grains. *Astrophys. J. Lett.* 768, L19.
- Liu, N., Gallino, R., Bisterzo, S., Davis, A.M., Savina, M.R., Pellin, M.J., 2014a. The  $^{13}\text{C}$ -pocket structure in AGB models: constraints from zirconium isotope abundances in single mainstream SiC grains. *Astrophys. J.* 788, 163.
- Liu, N., Savina, M.R., Davis, A.M., Gallino, R., Straniero, O., Gyngard, F., Pellin, M.J., Willingham, D.G., Dauphas, N., Pignatari, M., Bisterzo, S., Cristallo, S., Herwig, F., 2014b. Barium isotopic composition of mainstream silicon carbides from Murchison: constraints for s-process nucleosynthesis in asymptotic giant branch stars. *Astrophys. J.* 786, 66.
- Liu, N., Savina, M.R., Gallino, R., Davis, A.M., Bisterzo, S., Gyngard, F., Käppeler, F., Cristallo, S., Dauphas, N., Pellin, M.J., Dillmann, I., 2015. Correlated strontium and barium isotopic compositions of acid-cleaned single mainstream silicon carbides from Murchison. *Astrophys. J.* 803, 12.
- Lugaro, M., Davis, A.M., Gallino, R., Pellin, M.J., Straniero, O., Käppeler, F., 2003a. Isotopic compositions of strontium, zirconium, molybdenum, and barium in single presolar SiC grains and asymptotic giant branch stars. *Astrophys. J.* 593, 486–508.
- Lugaro, M., Herwig, F., Lattanzio, J.C., Gallino, R., Straniero, O., 2003b. s-Process nucleosynthesis in asymptotic giant branch stars: A test for stellar evolution. *Astrophys. J.* 586, 1305–1319.

- Lugaro, M., Karakas, A.I., Stancliffe, R.J., Rijs, C., 2012. The *s*-process in asymptotic giant branch stars of low metallicity and the composition of carbon-enhanced metal-poor stars. *Astrophys. J.* 747, 2.
- Lugaro, M., Tagliente, G., Karakas, A.I., Milazzo, P.M., Käppeler, F., Davis, A.M., Savina, M.R., 2014. The impact of updated Zr neutron-capture cross sections and new asymptotic giant branch models on our understanding of the *s* process and the origin of stardust. *Astrophys. J.* 780, 95.
- Lugaro, M., Zinner, E., Gallino, R., Amari, S., 1999. Si isotopic ratios in mainstream presolar SiC grains revisited. *Astrophys. J.* 527, 369–394.
- Maeder, A., 2009. Physics, formation and evolution of rotating stars. *Astronomy and Astrophysics Library*. Springer Berlin Heidelberg .
- Maeder, A., Meynet, G., 2014. Magnetic braking of stellar cores in red giants and supergiants. *Astrophys. J.* 793, 123.
- Massimi, C., et al., 2017. Neutron spectroscopy of  $^{26}\text{Mg}$  states: Constraining the stellar neutron source  $^{22}\text{Ne}(\alpha, n)^{25}\text{Mg}$ . *Physics Letters B* 768, 1–6.
- Merrill, P.W., 1952. Spectroscopic observations of stars of class S. *Astrophys. J.* 116, 21–26.
- Mosser, B., Goupil, M.J., Belkacem, K., Marques, J.P., Beck, P.G., Bloemen, S., De Ridder, J., Barban, C., Deheuvels, S., Elsworth, Y., Hekker, S., Kallinger, T., Ouazzani, R.M., Pinsonneault, M., Samadi, R., Stello, D., García, R.A., Klaus, T.C., Li, J., Mathur, S., Morris, R.L., 2012. Spin down of the core rotation in red giants. *Astron. Astrophys.* 548, A10.
- Nanni, A., Bressan, A., Marigo, P., Girardi, L., 2013. Evolution of thermally pulsing asymptotic giant branch stars - II. Dust production at varying metallicity. *Mon. Not. R. Astron. Soc.* 434, 2390–2417.
- Nittler, L.R., 2005. Constraints on heterogeneous galactic chemical evolution from meteoritic stardust. *Astrophys. J.* 618, 281–296.

- Nucci, M.C., Busso, M., 2014. Magnetohydrodynamics and deep mixing in evolved stars. I. Two- and three-dimensional analytical models for the asymptotic giant branch. *Astrophys. J.* 787, 141.
- Piersanti, L., Cristallo, S., Straniero, O., 2013. The effects of rotation on *s*-process nucleosynthesis in asymptotic giant branch stars. *Astrophys. J.* 774, 98.
- Pignatari, M., Herwig, F., Hirschi, R., Bennett, M., Rockefeller, G., Fryer, C., Timmes, F.X., Ritter, C., Heger, A., Jones, S., Battino, U., Dotter, A., Trappitsch, R., Diehl, S., Frischknecht, U., Hungerford, A., Magkotsios, G., Travaglio, C., Young, P., 2016. NuGrid stellar data set. I. Stellar yields from H to Bi for stars with metallicities  $Z = 0.02$  and  $Z = 0.01$ . *Astrophys. J. Suppl.* 225, 24.
- Pignatari, M., Wiescher, M., Timmes, F.X., de Boer, R.J., Thielemann, F.K., Fryer, C., Heger, A., Herwig, F., Hirschi, R., 2013. Production of carbon-rich presolar grains from massive stars. *Astrophys. J. Lett.* 767, L22.
- Rosenfield, P., Marigo, P., Girardi, L., Dalcanton, J.J., Bressan, A., Gullieuszik, M., Weisz, D., Williams, B.F., Dolphin, A., Aringer, B., 2014. Evolution of thermally pulsing asymptotic giant branch stars. IV. Constraining mass loss and lifetimes of low mass, low metallicity AGB stars. *Astrophys. J.* 790, 22.
- Siess, L., Goriely, S., Langer, N., 2004. Nucleosynthesis of *s*-elements in rotating AGB stars. *Astron. Astrophys.* 415, 1089–1097.
- Smith, V.V., Lambert, D.L., 1990. The chemical composition of red giants. III - Further CNO isotopic and *s*-process abundances in thermally pulsing asymptotic giant branch stars. *Astrophys. J. Suppl.* 72, 387–416.
- Speck, A.K., Thompson, G.D., Hofmeister, A.M., 2005. The effect of stellar evolution on SiC dust grain sizes. *Astrophys. J.* 634, 426–435.

- Spitoni, E., Romano, D., Matteucci, F., Ciotti, L., 2015. The effect of stellar migration on galactic chemical evolution: a heuristic approach. *Astrophys. J.* 802, 129.
- Spruit, H.C., 2002. Dynamo action by differential rotation in a stably stratified stellar interior. *Astron. Astrophys.* 381, 923–932.
- Srinivasan, B., Anders, E., 1978. Noble gases in the Murchison meteorite - Possible relics of s-process nucleosynthesis. *Science* 201, 51–56.
- Stephan, T., Trappitsch, R., Davis, A.M., Pellin, M.J., Rost, D., Savina, M.R., Yokochi, R., Liu, N., 2016. CHILI the Chicago Instrument for Laser Ionization a new tool for isotope measurements in cosmochemistry. *International Journal of Mass Spectrometry* 407, 1–15.
- Straniero, O., Gallino, R., Busso, M., Chiefei, A., Raiteri, C.M., Limongi, M., Salaris, M., 1995. Radiative  $^{13}\text{C}$  burning in asymptotic giant branch stars and s-processing. *Astrophys. J.* 440, L85–L87.
- Tagliente, G., et al., 2008a. Experimental study of the  $^{91}\text{Zr}(n,\gamma)$  reaction up to 26 keV. *Phys. Rev. C* 78, 045804.
- Tagliente, G., et al., 2008b. Neutron capture cross section of  $^{90}\text{Zr}$ : Bottleneck in the s-process reaction flow. *Phys. Rev. C* 77, 035802.
- Tagliente, G., et al., 2010. The  $^{92}\text{Zr}(n,\gamma)$  reaction and its implications for stellar nucleosynthesis. *Phys. Rev. C* 81, 055801.
- Takahashi, K., Yokoi, K., 1987. Beta-decay rates of highly ionized heavy atoms in stellar interiors. *Atomic Data and Nuclear Data Tables* 36, 375.
- Timmes, F.X., Clayton, D.D., 1996. Galactic evolution of silicon isotopes: application to presolar SiC grains from meteorites. *Astrophys. J.* 472, 723.
- Trappitsch, R., Stephan, T., Davis, A.M., Pellin, M.J., Savina, M.R., Gyngard, F., Bisterzo, S., Gallino, R., Dauphas, N., 2016. Iron and nickel isotopic



- compositions of presolar silicon carbide grains from AGB stars measured with CHILI. LPI Contributions 1921, 6515.
- Trippella, O., Busso, M., Palmerini, S., Maiorca, E., Nucci, M.C., 2016. s-Processing in AGB stars revisited. II. Enhanced  $^{13}\text{C}$  production through MHD-induced mixing. *Astrophys. J.* 818, 125.
- van Raai, M.A., Lugaro, M., Karakas, A.I., García-Hernández, D.A., Yong, D., 2012. Rubidium, zirconium, and lithium production in intermediate-mass asymptotic giant branch stars. *Astron. Astrophys.* 540, A44.
- Vassiliadis, E., Wood, P.R., 1993. Evolution of low- and intermediate-mass stars to the end of the asymptotic giant branch with mass loss. *Astrophys. J.* 413, 641–657.
- Ventura, P., D’Antona, F., 2005. Full computation of massive AGB evolution. I. The large impact of convection on nucleosynthesis. *Astron. Astrophys.* 431, 279–288.
- Ventura, P., Di Criscienzo, M., Carini, R., D’Antona, F., 2013. Yields of AGB and SAGB models with chemistry of low- and high-metallicity globular clusters. *Mon. Not. R. Astron. Soc.* 431, 3642–3653.
- Wallner, A., Bichler, M., Buczak, K., Dillmann, I., Käppeler, F., Karakas, A., Lederer, C., Lugaro, M., Mair, K., Mengoni, A., Schätzkel, G., Steier, P., Trautvetter, H.P., 2016. Accelerator mass spectrometry measurements of the  $^{13}\text{C}(\text{n},\gamma)^{14}\text{C}$  and  $^{14}\text{N}(\text{n},\text{p})^{14}\text{C}$  cross sections. *Phys. Rev. C* 93, 045803.
- Zinner, E., 2014. Presolar Grains, in: Davis, A.M., Exec. Eds. Holland, H.D., K., T.K. (Eds.), *Meteorites and Cosmochemical Processes*. Vol. 1 Treatise on Geochemistry, 2nd Ed. Elsevier, Oxford, pp. 181–213.